CHAPTER 99

FIELD MEASUREMENTS AND NUMERICAL MODELING OF HARBOR OSCILLATIONS DURING STORM WAVES

W. M. Jeong[1], J. W. Chae[2], W. S. Park[1], and K. T. Jung[2]

Abstract

A series of simultaneous field measurements for long and short-period waves under storm and calm wave conditions were made to understand harbor resonances in a partially enclosed harbor. During storm condition the frequency spectra show peaks of considerable magnitude around the wave period of 1 ~ 5 minutes, which are bounded long waves and their harmonics. They are strongly related with storm waves but longer period (free long) waves are not in the harbor. Numerical tests were also carried out by using the hybrid element model including entrance separation losses in a simple rectangular harbor to validate the model for a mostly constricted entrance case. Further the model was used to simulate the long period oscillation in Muko harbor. Comparisons were made between field data and numerical results to discuss the effect of storm waves on the long period oscillations. Tests demonstrate the effect of input parameters on model results and proper choice of them are stressed.

INTRODUCTION

Long-period wave oscillations in a harbor could create unacceptable vessel motions, excessive mooring forces and fender reactions leading to the breaking of mooring lines and fender system. The typical natural periods of a reasonable sized harbor or a moored vessel are of the order of magnitudes of minutes (Nagai *et al.*, 1994). One of the sources that generate the long-period waves of 2 ~ 3 minutes in the offshore side is the wave set-down travelling with the wave groups. In a partially enclosed harbor attacked by short waves through the narrow entrance, free long waves can be generated, and the waves further resonate the natural modes of the harbor basin (Mei and Agnon, 1989; Wu and Liu, 1990). Recently Girolamo (1996), and Okihiro and Guza (1996) showed that irregular short waves generate bounded long waves and free long waves which excite harbor resonance with extensive analyses of experimental and field measured data, respectively.

---

[1]Senior Research Scientist, Coastal Engineering Division, Korea Ocean Research & Development Institute, Ansan P.O. Box 29, Seoul 425-600, KOREA
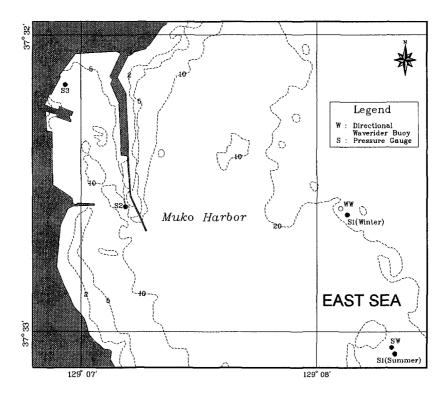
[2]Principal Research Scientist

Figure 1: Location map for field measurements around Muko harbor.

Most of previous studies are restricted to theoretical analysis with limited number of narrow frequency waves, and a few experimental and field measurement works taking into account irregular frequency-directional waves during storm conditions. As actual wind waves do not lie in a narrow frequency band, the resonance process is different. In order to investigate the effect of storm short waves to long-period harbor oscillations, a series of field measurements were conducted for both random sea waves and long-period waves inside and outside a small harbor. Harbor amplifications were calculated using HARBD linear model (Chen, 1986) including entrance loss and directional effects (Sand, 1982).

FIELD MEASUREMENTS AND ANALYSIS

Such phenomena of long-period oscillations were observed in the Muko harbor located at the east coast of Korea where north-eastern storm waves are dominant in winter season. The harbor is of a partially-enclosed rectangular shape with dimensions of 1 km long, 410 m wide, and entrance width of 250 m as shown in figure 1. The averaged water depth in the harbor is about 8.5 m.
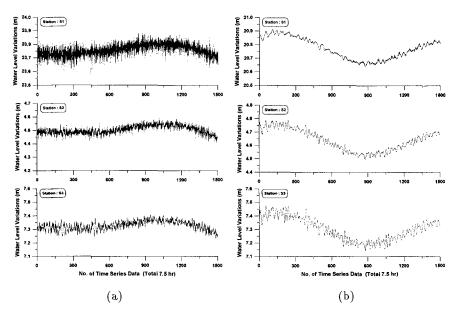
Figure 2: Time series of water level variations measured around Muko harbor; (a) Storm sea; (b) Calm sea.

Table 1: Characteristics of short- and long-period waves.

Data set no.	Starting time of measurement period in 1993	Periods of seiche at each station (min.)			Characteristics of measured short-period waves		
		S1	S2	S3	$\overline{H_{1/3}}$ (m)	$\overline{T_{H_{1/3}}}$ (sec)	Mean direction
1	03/18 15:10	23.1~28.2	11.1~28.2, 4.5, 3.6	11.1~12.2, 4.6, 3.4~3.6, 1.5~1.9	1.67	9.0	N55 ° E
2	03/20 01:18	28.2	13.4	13.4, 3.3~3.7	0.77	8.0	N56 ° E
3	07/07 15:00	18.0~27.8	12.3~20.4 (14.6)	11.4~14.6 (12.3)	0.35	4.0	N83 ° E
4	07/09 01:08	18.0~27.8	13.3~14.6, 5.8	13.3	0.43	4.4	N19 ° E
5	07/10 11:16	20.4~27.8	20.4, 13.3	11.4~13.3	0.37	5.2	N54 ° E

* Each record length is 34.1 hr.

** Shaded numeral denotes peak period corresponding to peak spectral density.
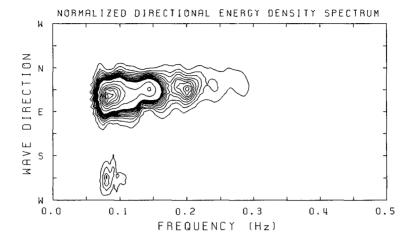
NORMALIZED DIRECTIONAL ENERGY DENSITY SPECTRUM

Figure 3: Typical directional spectrum of a short-period wave condition.

To investigate the relationship of short-period storm waves and long-period waves in a harbor, field measurements were performed at three reference stations as shown in figure 1. Using a Datawell directional waverider buoy short-period waves were measured at offshore stations WW and SW for 26.7 minutes at every hour in the interval of 0.78125 second. The frequency of the waves is in the range from 0.04 Hz (25 sec) to 0.25 Hz (4 sec). Using pressure-type wave gauges long-period waves were simultaneously measured at three stations S1, S2 and S3 (figure 1) for March $18 \sim 21$ and July $7 \sim 12$, 1993. Five sets of data (Table 1) were chosen for the analysis which show typical storm and calm wave conditions. Each set was recorded at 5 second intervals and recording length is approximately 34 hours. Typical time series of measured long-period waves for storm and calm sea conditions are presented in figure 2. It can be clearly found that the long period waves are amplified in a harbor and modulated with tide.

Directional-frequency spectra were obtained from the short-period wave analyses using Maximum Entropy Method (Kobune and Hashimoto, 1986), which show spreading of wave energy in both frequency and directional bands (figure 3). They are different from the narrow frequency banded waves used in the theoretical analysis. After filtering low-frequency waves from long-period wave signals using Butterworth high-pass filter in MATLAB, spectral analyses were made for each record of 4096 data points (at 30 second intervals averaged over 6 raw data). Standard spectral analysis based on FFT provides wave parameters and frequency spectrum that was herein obtained averaging over 16 raw harmonics. Two typical frequency spectra of storm and calm seas corresponding to time series of figure 2 in 128 frequency bands are shown in figure 4. Several peak frequency bands can be found around the wave period of $1 \sim 5$ minutes in the frequency spectrum for the storm wave condition, which may be resulted from group-bounded long waves and their harmonics resonated in the harbor (refer to Girolamo, 1996).
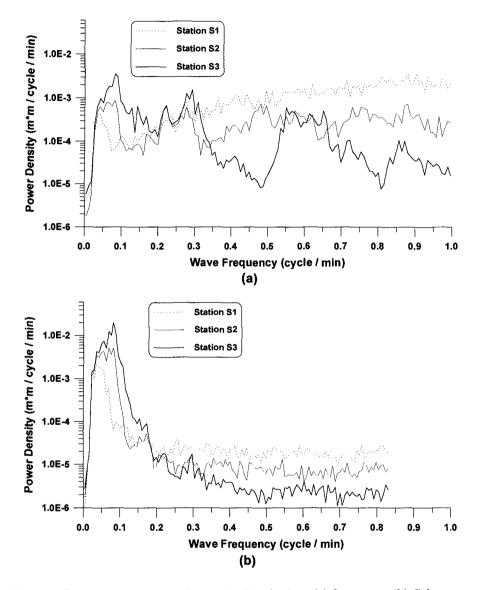
Figure 4: Power spectra measured around Muko harbor; (a) Storm sea; (b) Calm sea.

LONG-PERIOD WAVES AND HARBOR RESONANCE

Several resonant peaks are clearly seen in the frequency spectrum of long-period waves in the harbor when the storm waves occurred outside the harbor (figure 4(a)). However, only primary resonant peak can be seen in the calm sea condition (figure 4(b)). The observations reveal that long-period waves in the harbor are excited due to the nonlinear resonance by the groups of short waves.

On the basis of case studies of Wu and Liu (1990), it is possible to analyse approximately the characteristics of the oscillations. A little difference in the bounded long waves across the harbor mouth could generate free long waves of small amplitude in the neighbourhood of the first mode. But bounded long waves could be dominant at frequencies beyond the first mode because the harbor entrance is relatively large in comparison with the dimension of the harbor basin. The bounded long waves are mainly affected by short waves (swell) and resonated in the small harbor, but the first resonant mode and free long waves are not dependant on them. It is may be because of nonlinear energy dissipation in the harbor entrance even with the increase of the bounded long wave energy.

NUMERICAL MODELING

Mild slope equation of Berkhoff (1972) was adopted for simulating the harbor oscillations. There are three major energy dissipating processes in harbor resonance problem, i.e., bottom friction, energy absorption at solid boundaries, and entrance separation. Chen (1986) considered first two terms in his hybrid element model by introducing frictional loss parameter in governing equation and partial absorbing boundary condition. The governing equation and boundary conditions of Chen's model are summarized in figure 5. In the figure, ϕ is the complex-valued velocity potential in finite element region; ϕ^s is the velocity potential for scattered waves in the far field region; λ is the frictional parameter; α is a coefficient related to the wave reflection characteristics on solid boundaries; and C and C_g are celerity and group velocity, respectively.

Harbor Entrance Energy Loss

In this study, entrance separation losses were considered by introducing two matching conditions at the harbor mouth depicted as a dashed line in figure 6 as follows.

Continuity equation:
$$u_1 = u_2 = u_e \tag{1}$$

Dynamic equation:
$$\frac{p_1}{\rho} = \frac{p_2}{\rho} + \frac{1}{2} f_e u_e |u_e| + l \frac{\partial u_e}{\partial t} \tag{2}$$

in which u_1 and u_2 are water particle velocities in open sea region, A_1 and inner harbor region, A_2, respectively; u_e is the velocity of water particle at harbor entrance; f_e is loss coefficient; and l is the length of the jet flowing through the harbor mouth.

$$\lim_{r \to \infty} \sqrt{r} \left(\frac{\partial}{\partial r} - ik \right) \phi^s = 0$$

$$\nabla^2 \phi^s + k^2 \phi^s = 0$$

$$\frac{\partial \phi^s}{\partial n} = ika\phi^s$$

$$\nabla(\lambda CC_g \nabla \phi) + \frac{C_g}{C} \omega^2 \phi = 0$$
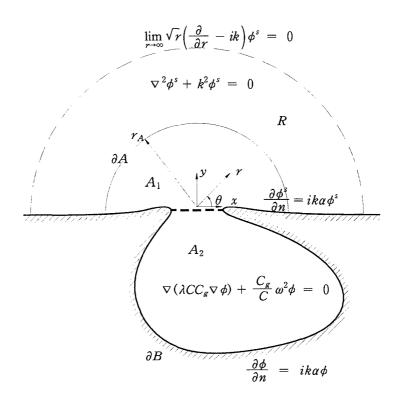
$$\frac{\partial \phi}{\partial n} = ika\phi$$

Figure 5: Hybrid element model, HARBD (Chen, 1986).

The second term of right hand side of equation (2) is generally nonlinear. To solve the boundary value problem efficiently in frequency domain, it should be linearized. Using Lorentz's transformation and averaging power along the water depth, it can be linearized as

$$\frac{1}{2} f_e u_e |u_e| \approx \gamma u_e \tag{3}$$

in which γ is the linearized loss coefficient including amplitude of water particle velocity at the interface of A_1 and A_2, which is given by

$$\gamma = \frac{4}{3\pi} f_e \bar{u}_e \frac{\sinh kh}{\cosh kh} \frac{2(5 + \cosh 2kh)}{3(2kh + \sinh 2kh)} \tag{4}$$

in which $\bar{u}_e$ is the amplitude of u_e; k is the incident wave number; and h is the depth of water.

Using complex valued velocity potential, the linearized matching conditions can be rewritten as

$$\frac{\partial \phi_1}{\partial n} = -\frac{\partial \phi_2}{\partial n} \tag{5}$$
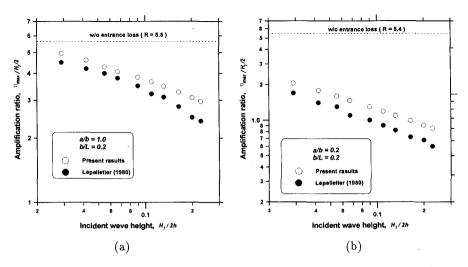
Figure 6: Variation of amplifications varying with incident wave heights; (a) fully opened case; (b) partially opened case.

$$\phi_1 = \phi_2 + \left(\frac{i\gamma}{\omega} + l\right) \frac{\partial \phi_2}{\partial n} \tag{6}$$

The entrance loss coefficient, f_e, are determined from the empirical formulation developed by Lepelletier (1980) given by

$$f_e = \begin{cases} CS & \text{for } S \leq 1 \\ C & \text{for } S \geq 1 \end{cases} \tag{7}$$

in which S is Stroul number $(=u_e/a\omega)$; C is empirical coefficient, 0.8 for fully opened harbor$(a/b = 1.0)$ and 1.15 for partially opened harbor $(a/b \leq 0.8)$; a is the width of entrance; and b is the width of harbor.

Comparison with Experimental Data

With reference to Lepelletier's (1980) laboratory tests a simple rectangular harbor was chosen for numerical calculation of amplification factors. The harbor bottom is flat and widths of the entrance gap are 0.2 (partially open) and 1.0 (fully open) times the harbor width. Using the values of K_r and β (discussed in Thompson et al., 1993), the modified Chen's model was run for the two cases (figure 6). The amplification factor is half as big as Lee's (1969). As shown in the figures the amplification factors taking into account of harbor entrance loss effects are resonably in good agreement with the data for the most constricted entrance case (figure 6(b)). It can be said that the linear model (HARBD) with linearization of nonlinear dissipation term due to flow separation in the harbor entrance will be a good tool for the estimation of the amplification of a restricted harbor. In case of Muko harbor the entrance energy loss may be not significant because the harbor is relatively wide opened.
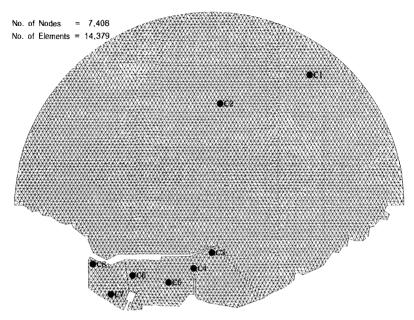
No. of Nodes   = 7,408
No. of Elements = 14,379

Figure 7: Finite element mesh for Muko harbor.

Model Application

The modified model was applied to calculate the harbor amplification due to group bounded and free long waves generated during the storm wave condition and resonated in the Muko harbor. Model boundary was taken large enough to cover offshore measurement station S1 as shown in figure 7. The water depth of far field area (analytic solution region in HARBD model) is assumed to be constant. Reflection coefficients vary from 0.95 (natural beach) to 0.99 (vertical sea wall) and also vary depending on the magnitude of frequency (i.e., from 0.4 for 15 sec to 0.98 for 180 sec waves at energy absorbing boundary). The numbers of triangular elements are 14379 and its size is small in order to resolve 30 sec period wave in water of 8.5 m depth. Numerical computation has been made for the 54 component waves of period range from 60 sec to 1400 sec Some comparison was made with experimental data. The amplification ratio is $\sqrt{S_i(f)/S(f)}$, where $S_i(f)$ is spectral density at the i-th point in the domain and $S(f)$ at offshore station. Figure 8 shows the amplification ratio at C7 (measurement station S3), and computation results are in reasonably good agreement with measured data, where water depth is chosen as mean depth of 17.2m. The water depth effects are dominant on the waves around the first resonant peak. The incident wave direction is also very important on the estimation of harbor amplification especially in high frequency range below 350 sec in Muko harbor (figure 9). Those wave periods are related with bounded long waves. Upon the test results of partial wave reflection (figure 10) the coefficient should vary depending on the wave length up to a certain wave period. With proper choice of parameters the modified numerical model performs reasonably well in relation to field data.
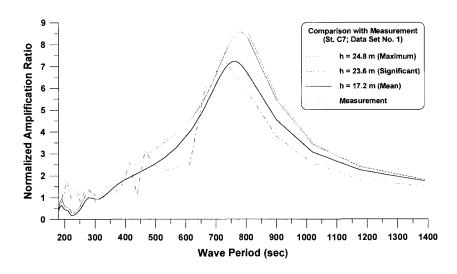
Figure 8: Comparison of normalized amplification ratios obtained by measurements and numerical calculation with various water depths in far field region.
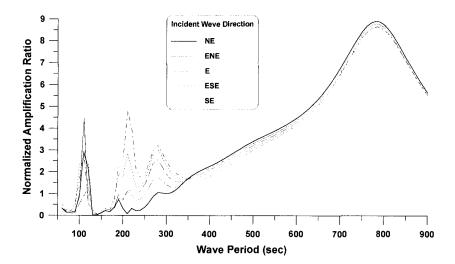

Figure 9: Variation of normalized amplifications with incident wave directions.
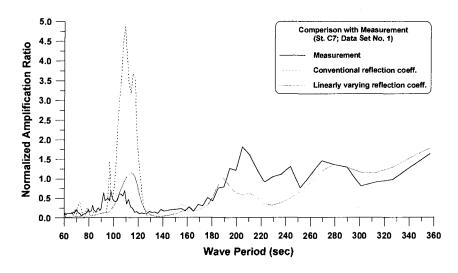
Figure 10: Comparison of normalized amplification ratios obtained by measurement and numerical calculation with different reflection coefficients.

CONCLUSIONS

Field measurements of short- and long-period waves were made to understand long-period oscillations generated by storm waves in a partially enclosed harbor. In a storm wave condition the frequency spectrum shows several resonant peaks, which are free long waves in the neighbourhood of the first mode, and bounded long waves and harmonics in the other modes. The bounded long waves are strongly dependant on short wind waves but the longer waves may be not. Chen's linear model was modified to cope with entrance energy losses due to flow separation. The model provided a good approximation to the harbor amplification of major resonant modes in the Muko harbor.

ACKNOWLEDGEMENTS

REFERENCES

Bowers, E. C. (1977). Harbor resonance due to set-down beneath wave groups. *J. Fluid Mech.*, **70**, 71-92.

Berkhoff, J. C. W. (1972). Computation of combined refraction and diffraction. *Proc., 13th Coast. Engrg. Conf.*, ASCE, New York, 471-490.

Chen, H. S. (1986). Effects of bottom friction and boundary absorption on water wave scattering. *Applied Ocean Research*, **8(2)**, 99-104.

Girolamo, P. D. (1996). An experiment on harbor resonance induced by incident regular waves and irregular short waves. *Coastal Engrg.*, **27**, 47-66.

Kobune, K. and N. Hashimoto. (1996). Estimation of directional spectra from the maximum entropy priciple. *Proc. 5th Int. Offshore Mech. and Arctic Engrg. Symp.*, ASME, **1**, 80-85.

Lee, J. J. (1969). Wave induced oscillations in harbors of arbitrary shape. *Report No. KH-R-20*, W. M. Keck Lab. of Hydraulics and Water Resources, Calif. Inst. of Technology, Pasadena, CA.

Lepelletier, T. G. (1980). Tsunamis-harbor oscillations induced by nonlinear transient long waves. *Report No. KH-R-41*, W. M. Keck Lab. of Hydraulics and Water Resources, Calif. Inst. of Technology, Pasadena, CA.

Mei, C. C. and Y. Agnon. (1989). Long-period oscillations in a harbor induced by incident short waves. *J. Fluid Mech.*, **208**, 595-608.

Nagai, T., N. Hashimoto, T. Asai, I. Tobiki, K. Ito, T. Toue, A. Kobayashi, and T. Shibata. (1994). Investigation of the harbor tranquility based on wavegroup characteristics. *HYDRO-PORT'94*, 203-215.

Okihiro, M. and R. T. Guza. (1996). Observations of seich forcing and amplification in three small harbors. *J. Wtrwy., Harb., Coast., Engrg., Div.*, ASCE, **122(5)**, 232-238.

Sand, S. E. (1982). Long waves in directional seas. *Coastal Engrg.*, **6**, 195-208.

Thompson, E. F. (1993). Numerical modeling of waves in harbors. *Waves'93*, 590-601.

Wu, J. K. and P. L.-F. Liu. (1990). Harbor excitations by incident wave groups. *J. Fluid Mech.*, **217**, 595-613.